# Mechanical Behaviour of Three Types of Stainless Steel After Exposure to Elevated Temperatures


***Zhong Tao*** [a]***, Xing-Qiang Wang*** [a,b]***, Md Kamrul Hassan*** [a]***, Tian-Yi Song*** [c]

*Centre for Infrastructure Engineering, Western Sydney University, Penrith, Australia*[(a)]

*Department of Civil Engineering, Shandong Polytechnic, Jinan, China*[(b)]

*College of Architecture and Civil Engineering, Beijing University of Technology, Beijing, China*[(c)]



## Abstract

Extensive studies have been conducted in the past to investigate the behaviour of stainless steel at ambient and elevated temperatures. In contrast, little information is available on its post-fire behaviour. In the present study, tensile tests were conducted on three types of stainless steel (i.e., austenitic, duplex and ferritic alloys) to determine their full-range stress–strain curves. Coupons extracted from the original sheet materials and the flat parts of square hollow sections were heated to various temperatures up to 1200 ºC and then cooled down to room temperature. The effects of temperature on different mechanical properties, including the elastic modulus, yield stress, ultimate strength, ultimate strain and strain hardening exponent, are analysed. Based on regression analysis, suitable modifications are made to an existing stress–strain model proposed by the authors for austenitic stainless steel in an earlier paper. After the modifications, the revised model can be applied to evaluate the post-fire behaviour of all the three types of stainless steel.



## Keywords

Stainless steel, Post-fire, Mechanical behaviour, Stress–strain models, Fracture.


## 1 Introduction

Stainless steel has been increasingly used in construction because of its excellent performance, such as corrosion resistance, aesthetic appearance and easy maintenance[1]. Generally, the grades of stainless steel can be categorised into five major groups on the basis of their crystalline structures. The most commonly used stainless steel materials in construction are austenitic, duplex and ferritic stainless steels, whereas martensitic and precipitation-hardening stainless steels have seldom been used as structural materials. Austenitic stainless steel typically contains 17–18% chromium and 8–11% nickel along with other elements, whereas duplex stainless steel is a type of alloy that typically contains a high chromium content of 22–23% and a moderate nickel content of 4–5%. In contrast, the most commonly used ferritic stainless steel has a content of 10.5–18% chromium and very little nickel[1,2]. Mechanical properties of stainless steel at room temperature have been extensively investigated and a number of stress–strain models have been proposed by Mirrambell and Real[3], Rasmussen[4], Gardner and Ashraf[5], Quach et al.[6], Tao and Rasmussen[7], and Arrayago et al.[8], respectively. Meanwhile, Mäkeläinen and Outinen[9], Chen and Young[10], and Gardner et al.[11,12] have experimentally investigated the elevated temperature material properties of stainless steel and a few stress–strain models are also available in the literature to account for the temperature effect[10–13].

Although extensive studies have been conducted in the past to investigate the behaviour of stainless steel at ambient and elevated temperatures, very little attention has been paid to its behaviour after exposure to elevated temperatures. Felicetti et al.[14] tested hot rolled and cold worked stainless steel bars (austenitic grade 1.4307) after exposed to elevated temperatures up to 850 °C. Their test results indicated that the fire-induced deterioration of cold worked bars was much more significant compared with their hot rolled counterparts after fire exposure. Wang et al.[15] conducted post-fire tests on flat, corner and curved coupons of austenitic grade 1.4301 steel. The test results indicated that the yield stresses of flat and curved coupons decreased somewhat when the temperature exceeded 500 °C. For corner coupons, the strength enhancement induced by cold forming reduced significantly with increasing temperature; the ductility recovered to some extent after the heat treatment. Meanwhile, a simplified stress–strain model has been developed by Wang et al.[15] for both flat and corner austenitic stainless steel after exposure to elevated temperatures and cooling to room temperature. However, Wang et al.'s model was developed only based on limited test data of a certain type of stainless steel. Obviously, more test data of austenitic stainless steel is required to further verify the capability of this model. Furthermore, no test data is available on other types of stainless steel after exposure to elevated temperatures, such as duplex and ferritic stainless steels.

In this paper, experimental results of a series of tensile tests are reported for three types of stainless steels (i.e., austenitic, duplex and ferritic stainless steels). The tensile coupons were extracted from the original sheet material and the flat parts of square hollow sections (SHS). Prior to the mechanical tests, these coupons had been heated to various temperatures up to 1200 ºC and then cooled down to room temperature. The effects of temperature on different mechanical properties are analysed. Based on regression analysis, Wang et al.'s model is further modified to predict the full-range stress–strain curves of all the three types of stainless steel.


Paper presented by Zhong Tao - Z.Tao@westernsydney.edu.au

## 2 Experimental Investigation

### 2.1 Preparation of stainless steel coupons

A total of five types of stainless steels, including two types of austenitic stainless steel (grades 1.4404 and 1.4307), two types of duplex stainless steel (grades 1.4362 and 1.4462), and one type of ferritic stainless steel (grade 1.4003), were selected for study in this paper. The chemical compositions of these stainless steel materials are shown in Table 1.

**Table 1. Chemical composition of stainless steels (%).**

| Steel type | Grade | C | Si | Mn | P | S | N | Cr | Cu | Mo | Ni |
|---|---|---|---|---|---|---|---|---|---|---|---|
| Austenitic | 1.4404 | 0.019 | 0.56 | 0.88 | 0.039 | <0.001 | 0.044 | 16.70 | – | 2.02 | 10.00 |
| | 1.4307 | 0.029 | 0.88 | 1.32 | 0.030 | 0.015 | – | 18.80 | – | – | 8.00 |
| Duplex | 1.4362 | 0.020 | 0.49 | 1.35 | 0.027 | 0.001 | 0.112 | 23.45 | 0.47 | 0.49 | 4.89 |
| | 1.4462 | 0.017 | 0.41 | 1.38 | 0.026 | 0.001 | 0.177 | 22.45 | – | 3.15 | 5.73 |
| Ferritic | 1.4003 | 0.008 | 0.70 | 1.12 | 0.021 | 0.002 | 0.015 | 11.20 | – | – | 0.58 |

Two types of steel coupons were prepared, including coupons extracted from the original sheet materials and coupons extracted from the flat parts of SHS tubes with a width of 150 mm. These tubes had been cold formed from the stainless steel parent sheet earlier. By comparing the test results of the two types of coupons, possible influence of cold forming process on the post-fire mechanical behaviour of stainless steel can be identified. It should be noted that the cold forming effect is only checked for the austenitic grade 1.4307 and ferritic grade 1.4003 stainless steels. Further research is required to investigate the influence of cold forming upon the subsequent post-fire performance of other types of stainless steel. All coupons were extracted along the rolling direction of the sheet. To avoid any heat influence when preparing the coupons, water-jet cutting was carried out. To fit in the furnace, the dimensions of the steel coupons are shown in Fig. 1. The nominal thicknesses of grades 1.4307 and 1.4003 are 3 mm, whereas other grades have a nominal thickness of 4 mm. The nominal width of all the coupons is 12.5 mm in the necking region. The actual thickness and width of each coupon were measured before the test to determine the cross-sectional area.

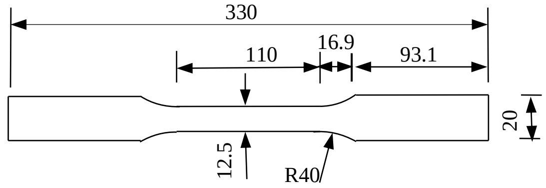


**Fig. 1. Dimensions of coupons (unit: mm).**

### 2.2 Testing procedure

A temperature-controlled furnace equipped with two thermocouples was used to heat treat the coupons. The target temperature ($T$) for the coupons ranged from 20 to 1200 °C, as shown in Tables 2–4 for different types of stainless steel. For similar tests of steel in the literature, the maximum $T$ selected was normally 1000 °C or less[15]. But in a real fire scenario, the environment temperature may exceed this limit. Therefore, a maximum $T$ of 1200 °C was chosen for grades 1.4307 and 1.4003 in this research to check the influence. Prior to conducting the tensile test, the stainless steel coupon was installed in the furnace for heat treatment. The furnace temperature was then increased to the pre-fix temperature $T$ at a heating rate of 20 °C/min. After reaching the target temperature, the furnace temperature was kept constant at $T$ for 30 min to ensure an even temperature distribution in the coupon. After the soak time of 30 min was reached, the furnace was turned off and the stainless steel coupon was cooled down to ambient temperature naturally. It should be noted that no load was applied to the stainless steel coupon during the heat treatment.

After the heat treatment, tensile tests were carried out using an Instron testing machine as shown in Fig. 2. An extensometer with a gauge length of 50 mm was mounted on the coupon to measure the extension. Strain rate control was used in accordance with the Australian standard AS 1391[16]. The initial strain rate was kept at 0.00025 /s until a strain of 0.1 was reached. Then the strain rate was increased to 0.001 /s until complete fracture of the sample. All test data were recorded automatically using a data logging system.

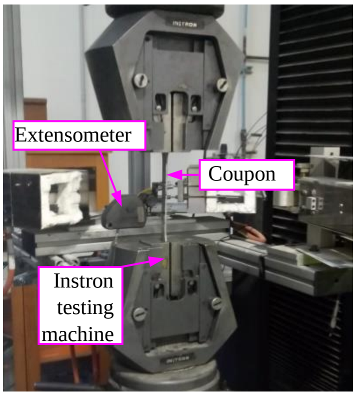


**Fig. 2. Tensile testing setup.**

## 3 Test Results and Discussion

The measured full-range stress–strain ($\sigma$–$\varepsilon$) curves are shown in Figs. 3–5 for the austenitic, duplex and ferritic alloys, respectively. The stress was calculated from the recorded load divided by the measured cross-sectional area of the coupon in the necking region, whereas the strain was determined based on the recordings of the extensometer. It is worth noting that the strength deterioration of the coupon became significant in the necking stage. Therefore, the determination of the fracture point (especially the corresponding modulus) is less accurate[17]. The measured mechanical properties of different types of stainless steel are presented in Tables 2–4, in which $T$ is the pre-fix temperature; $E_{sT}$ is the modulus of elasticity, $f_{yT}$ is the yield stress, $n_T$ is the strain hardening exponent; $f_{uT}$ and $\varepsilon_{uT}$ are the ultimate strength and corresponding ultimate strain, respectively; and $f_{fT}$, $\varepsilon_{fT}$ and $E_{fT}$ are the stress, strain and modulus at the fracture point, respectively. The subscript "T" in these parameters indicates that they are used for samples after exposure to elevated temperatures. But for consistency in analysing the test data, they are also used for samples without heat treatment ($T$ = 20 °C). However, the corresponding parameters denoted by $E_s$, $f_y$ $n$, $f_u$, $\varepsilon_u$, $f_f$, $\varepsilon_f$ and $E_f$, are specifically used for steel without heat treatment.

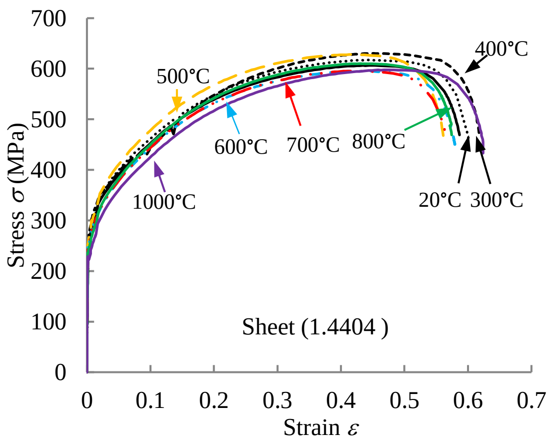


**(a) Grade 1.4404 (sheet)**

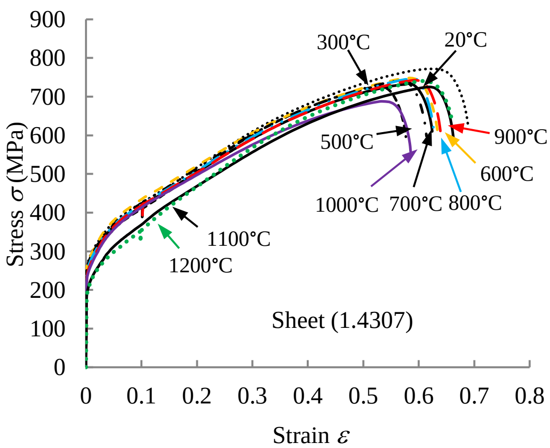


**(b) Grade 1.4307 (sheet)**

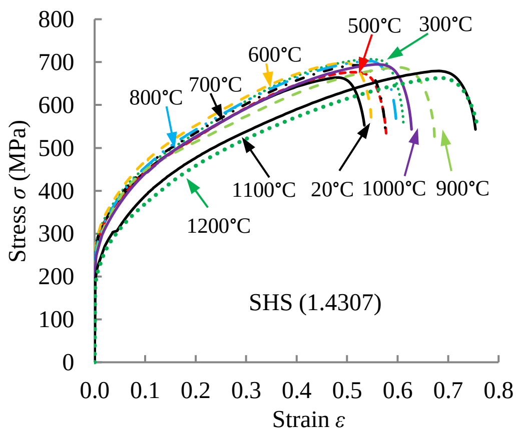


**(c) Grade 1.4307 (SHS flat)**

**Fig. 3. Stress–strain curves of austenitic stainless steel after elevated temperature exposure.**

As expected, the austenitic stainless steel shows significant strain-hardening, whereas the strain-hardening is less significant for both duplex and ferritic stainless steels. At room temperature, the yield stresses ($f_y$) of the two austenitic

Paper presented by Zhong Tao - Z.Tao@westernsydney.edu.au

grades are about 270 MPa, whereas those of the two duplex grades reach around 590 MPa. In contrast, the sheet material of the ferritic grade 1.4003 has a $f_y$–value of 331.6 MPa. The ultimate strengths ($f_u$) of the austenitic grades are above 600 MPa, which are comparable to those of the duplex grades. However, the ferritic grade has a much lower $f_u$, which is around 450 MPa. Furthermore, the deformation capacity of the austenitic grades is the highest, whereas those of the duplex and ferritic grades at room temperature are close to each other but much lower than that of the austenitic grades.

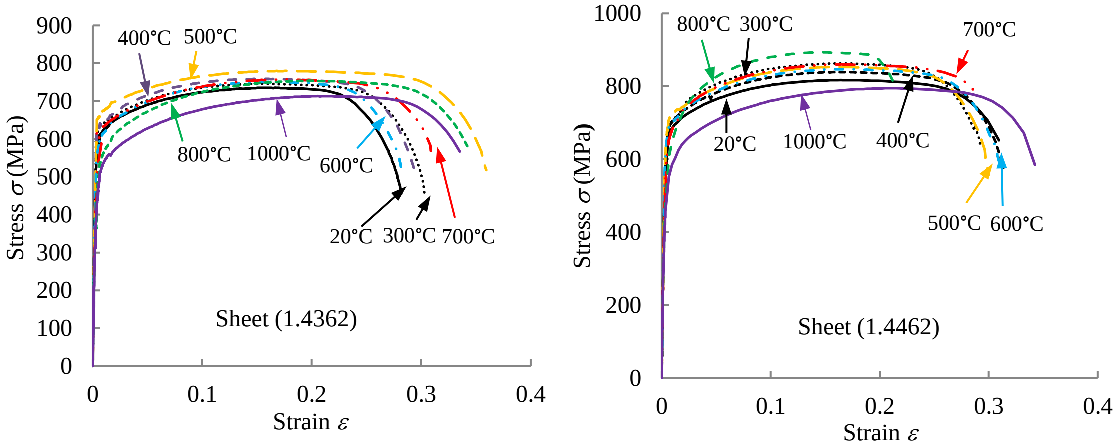


(a) Grade 1.4362 (sheet)

(b) Grade 1.4462 (sheet)

**Fig. 4. Stress–strain curves of duplex stainless steel after elevated temperature exposure.**

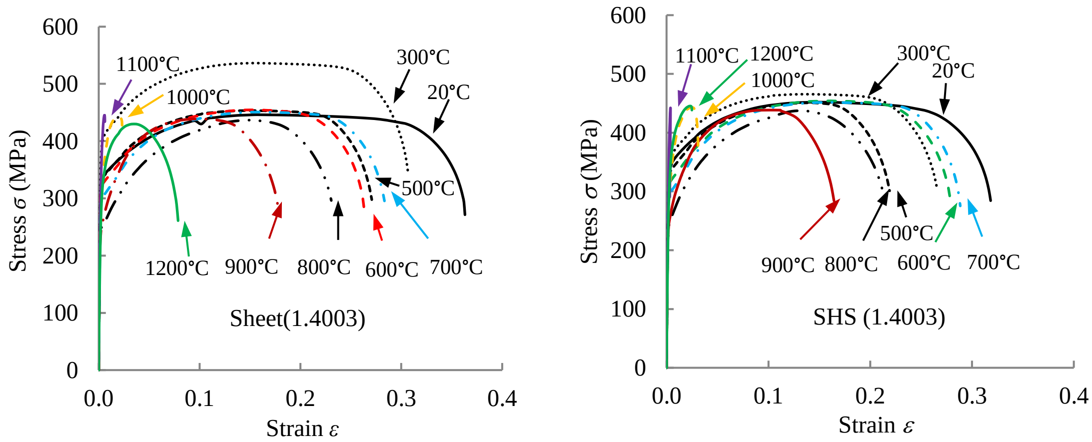


(a) Grade 1.4003 (sheet)

(b) Grade 1.4003 (SHS flat)

**Fig. 5. Stress–strain curves of ferritic stainless steel after elevated temperature exposure.**

**Table 2 Mechanical properties of austenitic stainless steel after exposure to elevated temperatures.**

| Coupon type | $T$ (°C) | $E_{sT}$ (MPa) | $f_{yT}$ (MPa) | $f_{uT}$ (MPa) | $n_T$ | $\varepsilon_{uT}$ | $f_{fT}$ (MPa) | $\varepsilon_{fT}$ | $E_{fT}$ (MPa) |
|---|---|---|---|---|---|---|---|---|---|
| Sheet (1.4404) | 20 | 191300 | 268.3 | 606.7 | 7.0 | 0.435 | 469.0 | 0.587 | 4900 |
| | 300 | 200200 | 258.0 | 617.2 | 8.0 | 0.440 | 463.0 | 0.601 | 4300 |
| | 400 | 210500 | 271.6 | 630.5 | 9.7 | 0.451 | 473.8 | 0.617 | 5900 |
| | 500 | 224100 | 264.4 | 628.2 | 15.8 | 0.418 | 468.0 | 0.561 | 6400 |
| | 600 | 200600 | 254.6 | 595.5 | 21.8 | 0.420 | 451.1 | 0.580 | 6900 |
| | 700 | 207000 | 254.0 | 595.9 | 16.0 | 0.428 | 461.9 | 0.567 | 5900 |
| | 800 | 194800 | 245.1 | 610.1 | 18.2 | 0.431 | 469.0 | 0.574 | 9900 |
| | 1000 | 229900 | 229.2 | 597.8 | 22.5 | 0.473 | 432.8 | 0.624 | 13800 |
| Sheet (1.4307) | 20 | 200500 | 265.3 | 735.9 | 14.6 | 0.582 | 610.2 | 0.624 | 8400 |
| | 300 | 206900 | 269.4 | 772.0 | 15.4 | 0.618 | 622.6 | 0.689 | 8800 |
| | 500 | 198700 | 257.4 | 726.2 | 22.6 | 0.533 | 596.3 | 0.577 | 8400 |
| | 600 | 214300 | 270.6 | 748.3 | 28.2 | 0.583 | 594.5 | 0.635 | 10300 |
| | 700 | 212500 | 265.2 | 740.8 | 24.7 | 0.562 | 597.8 | 0.614 | 10500 |
| | 800 | 196300 | 258.2 | 745.5 | 17.6 | 0.596 | 597.6 | 0.628 | 11400 |
| | 900 | 196200 | 247.1 | 742.9 | 16.0 | 0.593 | 611.3 | 0.639 | 9200 |
| | 1000 | 193400 | 240.3 | 687.9 | 20.4 | 0.533 | 558.1 | 0.585 | 10800 |
| | 1100 | 199400 | 199.3 | 725.2 | 17.2 | 0.619 | 593.9 | 0.662 | 9700 |
| | 1200 | 206100 | 196.6 | 740.7 | 14.0 | 0.612 | 628.8 | 0.661 | 6500 |
| SHS flat (1.4307) | 20 | 194300 | 274.9 | 664.0 | 10.1 | 0.485 | 552.4 | 0.534 | 6600 |
| | 300 | 201400 | 277.9 | 706.8 | 9.9 | 0.538 | 556.8 | 0.611 | 11000 |
| | 500 | 190500 | 269.5 | 676.5 | 11.2 | 0.509 | 532.9 | 0.577 | 10200 |
| | 600 | 208200 | 283.8 | 698.5 | 11.7 | 0.492 | 561.5 | 0.548 | 13800 |
| | 700 | 200000 | 270.1 | 692.5 | 14.3 | 0.509 | 536.5 | 0.576 | 12800 |
| | 800 | 206000 | 266.0 | 702.4 | 16.9 | 0.549 | 549.3 | 0.598 | 12700 |
| | 900 | 210100 | 252.9 | 688.1 | 16.3 | 0.601 | 514.2 | 0.673 | 15900 |
| | 1000 | 200200 | 245.4 | 694.7 | 16.9 | 0.556 | 543.1 | 0.628 | 10700 |
| | 1100 | 205100 | 204.5 | 679.5 | 16.3 | 0.682 | 543.0 | 0.754 | 6900 |
| | 1200 | 216100 | 193.0 | 663.0 | 15.3 | 0.689 | 549.0 | 0.758 | 4700 |

**Table 3 Mechanical properties of duplex stainless steel after exposure to elevated temperatures.**

| Coupon type | $T$ (°C) | $E_{sT}$ (MPa) | $f_{yT}$ (MPa) | $f_{uT}$ (MPa) | $n_T$ | $\varepsilon_{uT}$ | $f_{fT}$ (MPa) | $\varepsilon_{fT}$ | $E_{fT}$ (MPa) |
|---|---|---|---|---|---|---|---|---|---|
| Sheet (1.4362) | 20 | 230900 | 576.7 | 735.6 | 6.8 | 0.166 | 455.4 | 0.282 | 10500 |
| | 300 | 224200 | 619.5 | 746.1 | 6.4 | 0.160 | 445.3 | 0.303 | 14000 |
| | 400 | 248900 | 622.6 | 758.8 | 7.8 | 0.147 | 511.0 | 0.294 | 12700 |
| | 500 | 213800 | 655.9 | 780.0 | 7.1 | 0.168 | 517.5 | 0.359 | 9000 |
| | 600 | 216500 | 570.2 | 751.2 | 5.8 | 0.170 | 520.1 | 0.282 | 9300 |
| | 700 | 192200 | 527.5 | 757.3 | 4.9 | 0.172 | 568.5 | 0.309 | 7800 |
| | 800 | 190500 | 480.9 | 754.2 | 4.6 | 0.198 | 580.9 | 0.342 | 5100 |
| | 1000 | 195100 | 446.9 | 713.4 | 4.0 | 0.206 | 567.0 | 0.335 | 10100 |
| Sheet (1.4462) | 20 | 234800 | 600.3 | 817.2 | 6.9 | 0.164 | 651.8 | 0.309 | 5300 |
| | 300 | 212900 | 656.1 | 863.0 | 6.3 | 0.166 | 628.9 | 0.293 | 10800 |
| | 400 | 216500 | 661.1 | 839.2 | 6.9 | 0.158 | 576.2 | 0.315 | 10500 |
| | 500 | 227100 | 677.2 | 853.6 | 6.1 | 0.161 | 557.3 | 0.300 | 13300 |
| | 600 | 217100 | 660.3 | 847.3 | 6.7 | 0.172 | 596.0 | 0.310 | 11800 |
| | 700 | 217900 | 599.6 | 860.6 | 5.0 | 0.165 | 779.3 | 0.290 | 6200 |
| | 800 | 196300 | 530.6 | 893.3 | 5.7 | 0.152 | 815.8 | 0.213 | 5800 |
| | 1000 | 225400 | 483.3 | 794.6 | 4.8 | 0.218 | 584.7 | 0.342 | 8600 |

**Table 4 Mechanical properties of ferritic stainless steel after exposure to elevated temperatures.**

| Coupon type | $T$ (°C) | $E_{sT}$ (MPa) | $f_{yT}$ (MPa) | $f_{uT}$ (MPa) | $n_T$ | $\varepsilon_{uT}$ | $f_{fT}$ (MPa) | $\varepsilon_{fT}$ | $E_{fT}$ (MPa) |
|---|---|---|---|---|---|---|---|---|---|
| Sheet (1.4003) | 20 | 201100 | 331.6 | 446.1 | 8.2 | 0.155 | 271.5 | 0.363 | 10200 |
| | 300 | 226900 | 400.3 | 536.4 | 9.7 | 0.156 | 344.5 | 0.307 | 9300 |
| | 500 | 210200 | 335.2 | 453.4 | 19.6 | 0.151 | 297.8 | 0.263 | 7600 |
| | 600 | 210200 | 324.5 | 454.6 | 18.4 | 0.153 | 270.8 | 0.264 | 11400 |
| | 700 | 208500 | 302.2 | 451.0 | 27.2 | 0.165 | 295.6 | 0.283 | 7100 |
| | 800 | 207900 | 250.3 | 436.7 | 31.3 | 0.152 | 296.4 | 0.231 | 6100 |
| | 900 | 200200 | 254.0 | 439.8 | 10.7 | 0.107 | 288.2 | 0.178 | 7200 |
| | 1000 | 204300 | 323.2 | 442.8 | 7.9 | 0.019 | 427.8 | 0.023 | 13100 |
| | 1100[a] | 200500 | 322.8 | 445.2 | 6.0 | 0.006 | – | – | – |
| | 1200 | 170000 | 322.4 | 429.9 | 4.7 | 0.037 | 261.1 | 0.079 | 12700 |
| SHS flat (1.4003) | 20 | 191800 | 339.9 | 452.0 | 9.8 | 0.150 | 284.4 | 0.318 | 7700 |
| | 300 | 191000 | 352.3 | 465.5 | 7.8 | 0.135 | 305.3 | 0.266 | 6800 |
| | 500 | 201100 | 333.7 | 450.9 | 15.0 | 0.144 | 301.0 | 0.219 | 6900 |
| | 600 | 214500 | 316.1 | 454.2 | 14.7 | 0.161 | 281.5 | 0.279 | 8400 |
| | 700 | 219000 | 298.2 | 451.7 | 26.7 | 0.161 | 275.4 | 0.288 | 9600 |
| | 800 | 194200 | 249.8 | 437.8 | 17.2 | 0.134 | 284.5 | 0.214 | 6100 |
| | 900 | 207100 | 254.8 | 438.4 | 12.2 | 0.112 | 284.1 | 0.164 | 8100 |
| | 1000 | 201100 | 314.3 | 443.1 | 8.3 | 0.025 | 377.3 | 0.031 | 16300 |
| | 1100[a] | 203000 | 333.0 | 442.0 | 6.1 | 0.004 | – | – | – |
| | 1200[a] | 180500 | 352.0 | 445.0 | 4.8 | 0.024 | – | – | – |

[a] Values of $f_{\mathrm{fT}}$, $\varepsilon_{\mathrm{fT}}$ and $E_{\mathrm{fT}}$ are not available due to brittle fracture.

When the temperature is 500 °C or lower, its influence on the $\sigma$–$\varepsilon$ curve is negligible for all stainless steel grades, which can be observed from the $\sigma$–$\varepsilon$ curves shown in Figs. 3–5. But the influence becomes obvious when the temperature reaches 600 °C or higher. Fig. 6 shows the $\sigma$–$\varepsilon$ curves of austenitic grade 1.4404, duplex grade 1.4362 and ferritic grade 1.4003 stainless steels corresponding to temperatures of 20 °C and 1000 °C, respectively. All these $\sigma$–$\varepsilon$ curves are for coupons extracted from the original sheet materials. As can be seen, the austenitic stainless steel at room temperature is more ductile than the duplex and ferritic stainless steels. After exposure to 1000 °C, the shape of the $\sigma$–$\varepsilon$ curves has not significantly changed for the austenitic and duplex stainless steels. Despite this, there are a reduction in yield stress and an increase in fracture strain for the two types of materials. But on the contrary, the yield stress of the ferritic stainless steel at $T$ of 1000 °C shows a recovery back to its yield stress at ambient temperature. Meanwhile, there is a significant reduction in the fracture strain corresponding to the fracture point, indicating a very brittle failure after exposure to 1000 °C. The comparison highlights the difference in mechanical behaviour for different types of stainless steel after exposure to elevated temperatures. A more detailed analysis will be conducted in Section 5 to investigate the effects of heat exposure on different mechanical properties of stainless steel.

The influence of cold forming procedure is investigated on the austenitic grade 1.4307 and ferritic grade 1.4003 stainless steels. Its effect on the yield stress $f_{\mathrm{yT}}$ is shown in Fig. 7, whereas Fig. 8 demonstrates the effect of cold forming on the ultimate strain $\varepsilon_{\mathrm{uT}}$ corresponding to the ultimate strength $f_{\mathrm{uT}}$. For coupons extracted from the middle part of the plates of the finished SHSs, obvious cold forming effect can still be observed for the austenitic stainless steel. At room temperature, a slight increase of 3.6% in yield stress is induced by cold forming of this material. However, cold forming leads to a significant reduction in both ultimate strength $f_{\mathrm{u}}$ and corresponding ultimate strain $\varepsilon_{\mathrm{u}}$; the corresponding reductions are 9.8% and 16.7%, respectively. When $T$ reaches 900 °C or above, the mechanical properties of the cold formed austenitic stainless steel become close to those of the parent material, indicating the diminishing of the cold forming effect. This is consistent with the observation reported earlier for austenitic stainless steel corner coupons[15]. However, no obvious cold forming effect is found for the ferritic stainless steel flat coupons despite that this effect has been observed in ferritic stainless steel corner coupons[7]. As shown in Fig. 7, the ferritic stainless steel sheet has a much higher yield stress at $T$ of 300 °C than that of the flat coupon extracted from the SHS section. This is likely due to test error, which needs further clarification.

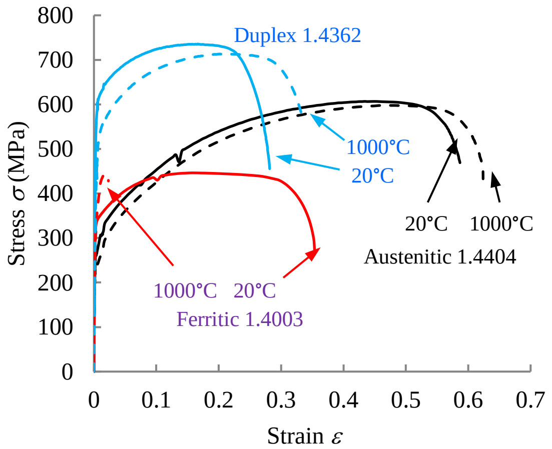


**Fig. 6. Influence of $T$ on $\sigma$–$\varepsilon$ curves of stainless steel.**

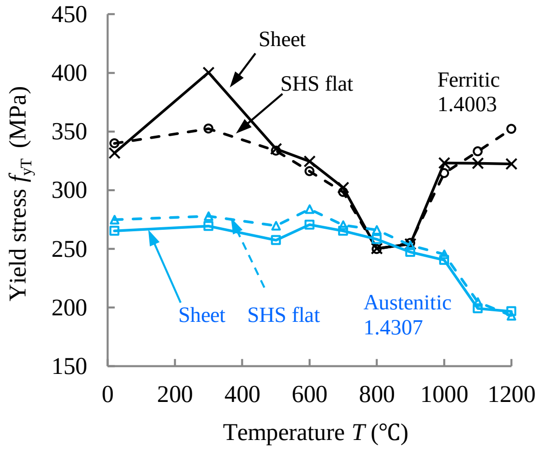


**Fig. 7. Influence of cold forming on yield stress.**

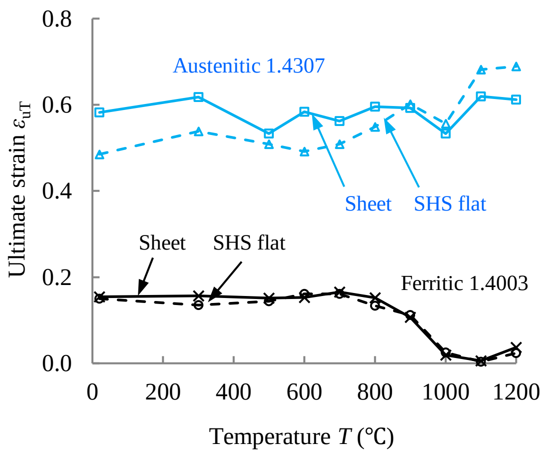


**Fig. 8. Influence of cold forming on ultimate strain.**

# 4 Expression of Stress–strain Relationship for Post-fire Stainless Steel

## 4.1 Existing stress–strain model

Rasmussen[4] proposed a full-range $\sigma$–$\varepsilon$ model containing two stages for room temperature stainless steel based on a large amount of test data; this model was later adopted in EN 1993-1-4[18]. Rasmussen's model was modified by Wang et al.[15] to represent the $\sigma$–$\varepsilon$ relationship of austenitic stainless steel after exposure to elevated temperatures. The revised model is expressed by Eqs. (1) to (4).

$$\varepsilon=\begin{cases}\dfrac{\sigma}{E_{\mathrm{sT}}}+0.002\left(\dfrac{\sigma}{f_{\mathrm{yT}}}\right)^{n_{\mathrm{T}}} & \sigma\le f_{\mathrm{yT}} \quad (1a)\\ 0.002+\dfrac{f_{\mathrm{yT}}}{E_{\mathrm{sT}}}+\dfrac{\sigma-f_{\mathrm{yT}}}{E_{\mathrm{yT}}}+\varepsilon_{\mathrm{uT}}\left(\dfrac{\sigma-f_{\mathrm{yT}}}{f_{\mathrm{uT}}-f_{\mathrm{yT}}}\right)^{m_{\mathrm{T}}} & f_{\mathrm{yT}}<\sigma\le f_{\mathrm{uT}} \quad (1b)\end{cases}$$

$$n_{\mathrm{T}}=\frac{ln(20)}{ln(\frac{f_{\mathrm{yT}}}{f_{0.01\mathrm{T}}})} \tag{2}$$

$$E_{\mathrm{yT}}=\frac{E_{\mathrm{sT}}}{1+0.002n_{\mathrm{T}}E_{\mathrm{sT}}/f_{\mathrm{yT}}} \tag{3}$$

$$m_{\mathrm{T}}=1+3.5\frac{f_{\mathrm{yT}}}{f_{\mathrm{uT}}} \tag{4}$$

where $f_{0.01\mathrm{T}}$ is the 0.01% proof yield stress, $E_{\mathrm{yT}}$ is the modulus at the onset of the second stage, and $m_{\mathrm{T}}$ is the strain hardening exponent in this stage. The corresponding parameters for steel without exposure to elevated temperature are designated by $f_{0.01}$, $E_{\mathrm{y}}$ and $m$, respectively.

Five key parameters, including $E_{\mathrm{sT}}$, $f_{\mathrm{yT}}$, $f_{\mathrm{uT}}$, $n_{\mathrm{T}}$, and $\varepsilon_{\mathrm{uT}}$, need to be determined for the above model. Wang et al.[15] conducted tests on austenitic grade 1.4301 stainless steel exposed to various temperatures (200–1000 °C). From the limited test data, they found that only $f_{\mathrm{yT}}$ shows an obvious trend of decrease when the temperature is higher than 500 °C, whereas other parameters generally remained unchanged compared with the corresponding values at room temperature. Accordingly, Eqs. (5)–(9) were proposed by Wang et al.[15] to calculate $f_{\mathrm{yT}}$, $E_{\mathrm{sT}}$, $f_{\mathrm{uT}}$, $n_{\mathrm{T}}$, and $\varepsilon_{\mathrm{uT}}$, respectively.

$$\frac{f_{\mathrm{yT}}}{f_{\mathrm{y}}}=\begin{cases}1 & T\le 500\ ℃\\ 1-1.75\times10^{-4}(T-500)-2.71\times10^{-7}(T-500)^2 & T>500\ ℃\end{cases} \tag{5}$$

$$\frac{E_{\mathrm{sT}}}{E_{\mathrm{s}}}=1 \tag{6}$$

$$\frac{f_{\mathrm{uT}}}{f_{\mathrm{u}}}=1 \tag{7}$$

$$\frac{n_{\mathrm{T}}}{n}=1 \tag{8}$$

$$\frac{\varepsilon_{\mathrm{uT}}}{\varepsilon_{\mathrm{u}}}=1 \tag{9}$$

As described in Section 3, this paper provides not only new test data pertaining to the post-fire behaviour of austenitic stainless steel, but also new test data covering duplex and ferritic stainless steels. Wang et al.'s model[15] will be assessed using the new test data, and suitable modifications, if necessary, will be made. In addition, Wang et al.'s model does not have a necking stage. Steel fracture may be of great interest to design engineers since a structure is likely to develop large deformation during fire exposure. Therefore, Wang et al.'s model is also revised in this paper to include a necking stage.

## 4.2 Revised stress–strain model

As shown in Fig. 9, the original model proposed by Wang et al.[15] only predicts $\sigma$–$\varepsilon$ relationship up to the ultimate strain $\varepsilon_{\mathrm{uT}}$. This model is revised to include a post-peak stage BC to represent necking and fracture, whereas stages OA and AB remain unchanged. It is observed that the shape of the post-peak stage of stress–strain curves plotted in Figs. (3)–(5) is quite similar to that of the strain-hardening stage of mild steel, except that the strain-hardening curve of mild steel is an ascending curve. Based on this observation, the expression describing the strain-hardening behaviour of mild steel proposed by Tao et al.[19] is adopted herein to represent the post-peak stage of stainless steel, as expressed by Eq. (10c), where $p$ in this equation is the strain softening exponent, determined by Eq. (11).

Meanwhile, the expressions of $n_{\mathrm{T}}$, $E_{\mathrm{yT}}$ and $m_{\mathrm{T}}$ remain unchanged. Similarly, the expressions of Eqs. (1a) and (1b) are still used in the revised model to represent stages 1 and 2, respectively, except the replacement of $\varepsilon_{\mathrm{uT}}$ in Eq. (1b) with $\varepsilon_{\mathrm{upT}}$ expressed by Eq. (12). The revised equation is given by Eq. (10b) to represent the second stage (AB) of the $\sigma$–$\varepsilon$ relation, as shown in Fig. 9. When developing the $\sigma$–$\varepsilon$ model for room temperature stainless steel, Rasmussen[4] simplified the expression for the second stage by arguing that the error could be ignored since stainless steel is generally ductile. Wang et al.[15] continued to use the simplified expression proposed by Rasmussen[4]. This simplification, however, will generally lead to an overestimation of the ultimate strain $\varepsilon_{\mathrm{uT}}$ in the predicted curve. The larger the yield stress and the larger the strain-hardening effect, the greater is the overestimation of $\varepsilon_{\mathrm{uT}}$. For the current test results, it is found that the prediction error in $\varepsilon_{\mathrm{uT}}$ resulting from this simplification ranges from 5.0% to 19.6%. The test curve of austenitic 1.4307 sheet exposed to a temperature of 1100 °C is shown in Fig. 10 as an example. To eliminate the prediction errors resulting from any input parameters, only measured results of various parameters presented in Table 2 are used to generate the $\sigma$–$\varepsilon$ relation. As can be seen in Fig. 10, the ultimate strain is overestimated by 15.5% when Eq. (1b) is used. In contrast, the $\sigma$–$\varepsilon$ curve passes through the actual peak point when Eq. (10b) is used instead for prediction. This comparison justifies the proposed revision to Eq. (1b), which also facilitates the inclusion of a post-peak stage in the model.

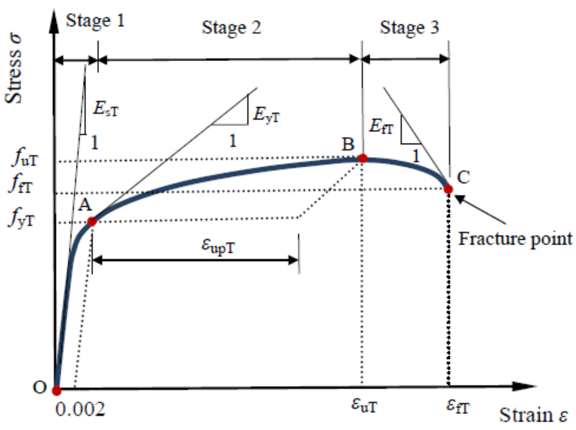


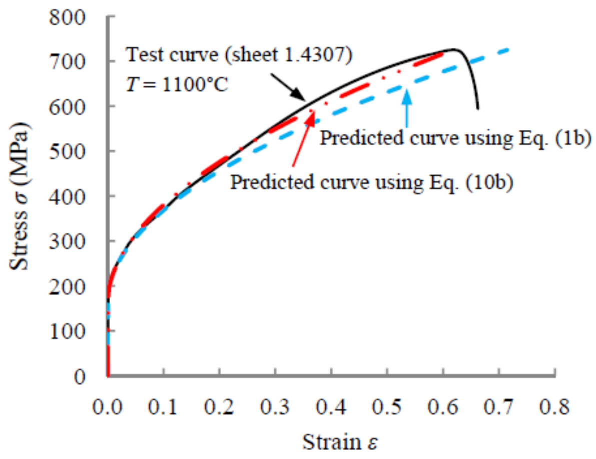


**Fig. 9. Revised stress–strain model.** **Fig. 10. Comparison of predictions using Eqs. (1b) and (10b).**

It should be noted that a total of 8 key parameters are required by Eq. (10) to generate a full-range $\sigma$–$\varepsilon$ curve with a necking stage. These parameters are the modulus of elasticity $E_{sT}$, yield stress $f_{yT}$, ultimate strength $f_{uT}$, strain hardening exponent $n_T$, ultimate strain $\varepsilon_{uT}$, fracture stress $f_{fT}$, fracture strain $\varepsilon_{fT}$ and the modulus at fracture point $E_{fT}$. From the measured full-range stress–strain curves shown in Figs. 3–5, all these key parameters have been obtained and presented in Tables 2–4. These parameters may be functions of exposed temperature and material properties at ambient temperature. Based on the test data, a statistic analysis is carried out as follows to derive simple equations to predict these key parameters in Eq. (10).

$$\varepsilon = \begin{cases} \frac{\sigma}{E_{sT}} + 0.002\left(\frac{\sigma}{f_{yT}}\right)^{n_T} & \sigma \le f_{yT} \quad (10a) \\ 0.002 + \frac{f_{yT}}{E_{sT}} + \frac{\sigma - f_{yT}}{E_{yT}} + \varepsilon_{upT}\left(\frac{\sigma - f_{yT}}{f_{uT} - f_{yT}}\right)^{m_T} & f_{yT} < \sigma \le f_{uT} \quad (10b) \\ \varepsilon_{uT} + (\varepsilon_{fT} - \varepsilon_{uT})\left(\frac{\sigma - f_{uT}}{f_{fT} - f_{uT}}\right)^{p} & f_{fT} \le \sigma < f_{uT} \quad (10c) \end{cases}$$

$$p = \frac{f_{uT} - f_{fT}}{E_{fT}(\varepsilon_{fT} - \varepsilon_{uT})} \quad \text{(but } \le 1\text{)} \qquad (11)$$

$$\varepsilon_{upT} = \varepsilon_{uT} - 0.002 - \frac{f_{yT}}{E_{sT}} - \frac{f_{uT} - f_{yT}}{E_{yT}} \qquad (12)$$

## 5 Determination of Key Parameters

Due to limited availability of test data, these of flat coupons reported by Wang et al.[15] for austenitic stainless steel are combined with the current test data for developing a more robust $\sigma$–$\varepsilon$ model. Unless otherwise specified, the default source of the test data is from the current test program. When analysing the influence of temperature on different parameters in the following subsections, it is found that there is no need to differentiate the sheet material and that extracted from the SHS.

### 5.1 Modulus of elasticity $E_{sT}$ and ultimate strength $f_{uT}$

The experimental values of $E_{sT}/E_s$ and $f_{uT}/f_u$ are depicted in Figs. 11 and 12, respectively, as a function of temperature $T$. It seems that the steel type has no obvious influence on the measured values of $E_{sT}/E_s$ or $f_{uT}/f_u$. Meanwhile, $E_{sT}$ and $f_{uT}$ remain unchanged even when the exposed temperature reaches 1200 °C. This is consistent with the previous observation reported by Wang et al.[15]. Therefore, Eqs. (6) and (7) can not only be used for austenitic stainless steel but also for duplex and ferritic stainless steels. It should be noted that the variation in $E_{sT}/E_s$ is much more significant than that in $f_{uT}/f_u$. This is probably associated with the low accuracy of elastic modulus measurement using extensometers, which might be improved if strain gauges were used instead.

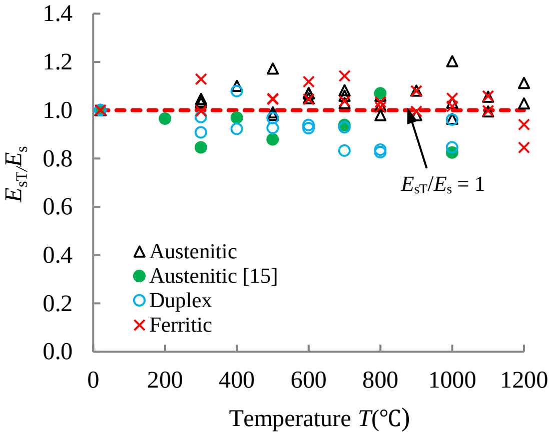


**Fig. 11.** $E_{sT}/E_s$ **versus** $T$ **for all grades.**

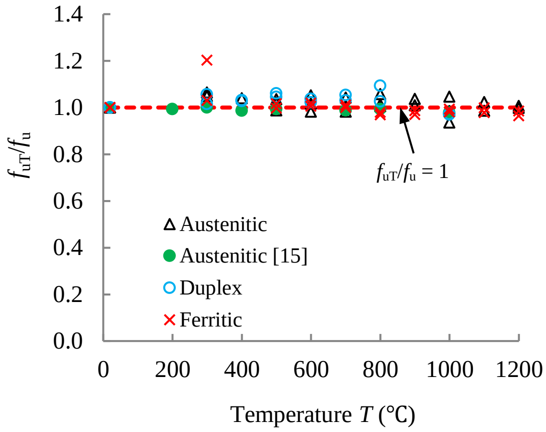


**Fig. 12.** $f_{uT}/f_u$ **versus** $T$ **for all grades.**

## 5.2 Yield stress $f_{yT}$ and ultimate strain $\varepsilon_{uT}$

Figs. 13 and 15 illustrate the ratios of $f_{yT}/f_y$ and $\varepsilon_{uT}/\varepsilon_u$, respectively, for austenitic and duplex stainless steels; while the two ratios for ferritic stainless steel are shown in Figs. 14 and 16, respectively. In general, if the temperature is 500 °C or lower, the residual yield stress $f_{yT}$ of austenitic stainless steel does not obviously change although some fluctuations can be seen. This is consistent with the previous observation reported by Wang et al.[15]. However, for the duplex and ferritic stainless steels, $f_{yT}$ increases to some extent when $T$ is between 300 and 500 °C. This is accompanied by a slight decrease in ductility. Previous investigations[20–22] indicate that in the temperature range of 280–500 °C, ferrite decomposes to chromium-rich phase α′ and iron-rich phase α; the decomposition and grain growth lead to embrittlement of the duplex or ferritic alloy. Since the embrittlement reaches its highest rate at 475 °C, this phenomenon is called 475 °C embrittlement by some researchers[22]. In the current test, the soak time was relatively short (30 min). This may explain the minor impact of embrittlement in this temperature range; the influence is not considered in the following model development.

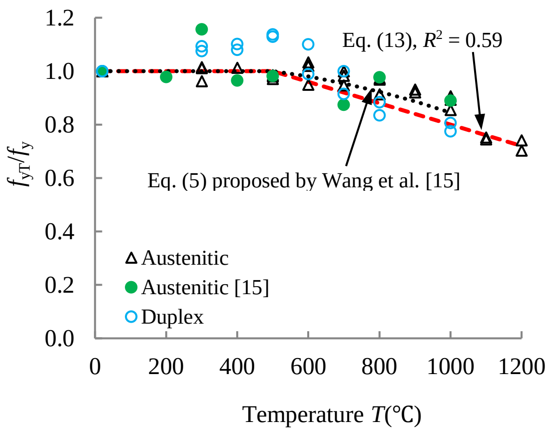


**Fig. 13.** $f_{yT}/f_y$ **versus** $T$ **for austenitic and duplex stainless steels.**

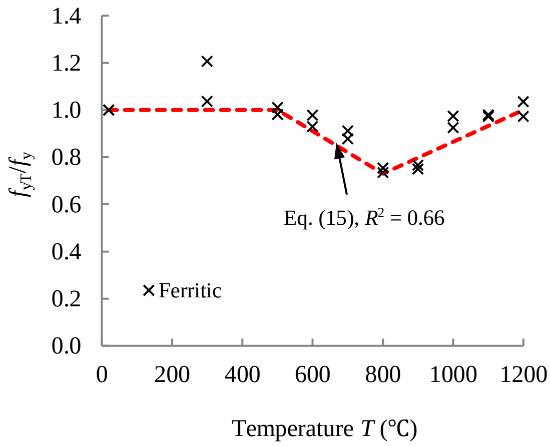


**Fig. 14.** $f_{yT}/f_y$ **versus** $T$ **for ferritic stainless steel.**

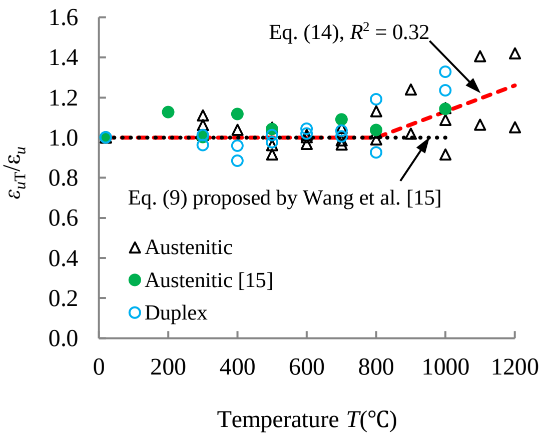


**Fig. 15.** $\varepsilon_{uT}/\varepsilon_u$ **versus** $T$ **for austenitic and duplex stainless steels.**

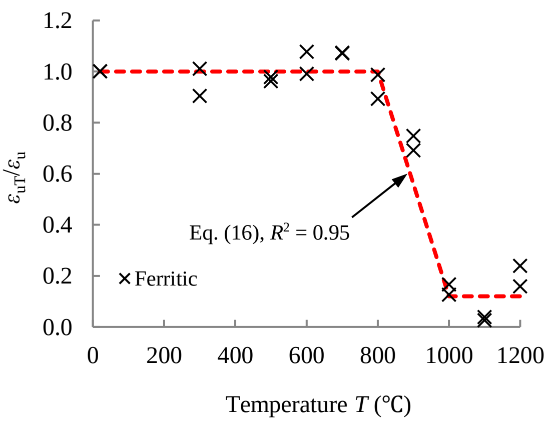


**Fig. 16.** $\varepsilon_{uT}/\varepsilon_u$ **versus** $T$ **for ferritic stainless steel.**

When the temperature exceeds 500 °C, the yield stress $f_{yT}$ of austenitic and duplex grades decreases continuously with increasing temperature, as shown in Fig. 13. A reduction of 25.9% in yield stress is observed for the sheet of austenitic grade 1.4307 when $T$ = 1200 °C. It is interesting to note that the yield stress of ferritic stainless steel also decreases once $T$ exceeds 500 °C, as shown in Fig. 14. But the lowest yield stress occurs when $T$ = 800 °C and the corresponding strength reduction is about 25% compared with the yield stress at room temperature. When $T$ exceeds 800 °C, the yield stress rises again with increasing temperature. After exposure to a $T$ of 1100 °C, the yield stress has almost fully recovered to $f_y$ at ambient temperature.

As shown in Figs. 15 and 16, the ultimate strain has not been significantly affected by $T$ for all grades until $T$ exceeds 800 °C. Although Wang et al.[15] suggested a higher temperature limit of 1000 °C for austenitic stainless steel, the combined test data of austenitic and duplex alloys seem to suggest an increase in ultimate strain beyond 800 °C despite the obvious variation in test data. On the contrary, $\varepsilon_{uT}$ of the ferritic stainless steel drops dramatically to around 14% of $\varepsilon_u$ when $T$ = 1000 °C; no obvious recovery can be found beyond this temperature. This embrittlement of the ferritic stainless steel can be clearly seen from the $\sigma$–$\varepsilon$ curves shown in Fig. 5. For ferritic grade1.4003, its chromium content is normally around 10.5–12.5%[2] and the material used in the current test program has a corresponding value of 11.2%. It is reported that the austenite γ in the dual phase region (δ+γ) might be transformed to martensite when the material is heated to over 880 °C and cools down relatively quick in air[23,24]; detrimental precipitates may also be formed during cooling[21]. Both factors can contribute to embrittlement of the steel after the heat treatment. In the current test, only a length of 65 mm in the middle part of the steel coupon was exposed to heat. The corresponding cooling rate (40–120 °C/min) was relatively high for the sample after the furnace was turned off. This might explain the abrupt reduction in $\varepsilon_{uT}$ when $T$ is 900 °C or above. Further research on microstructure of ferritic stainless steel after elevated temperature exposure is still required to clarify this.

In general, austenitic and duplex stainless steels have similar $f_{yT}/f_y$ and $\varepsilon_{uT}/\varepsilon_u$ ratios at a certain $T$, as shown in Figs. 13 and 15. Therefore, same equations may be used for them to predict $f_{yT}$ and $\varepsilon_{uT}$. But different equations should be developed for ferritic stainless steel because of the difference in behaviour. Eq. (6) originally proposed by Wang et al.[15] is tentatively used to predict $f_{yT}$ of austenitic and duplex stainless steels, and the results are shown in Fig. 13. It seems that the predictions of $f_{yT}$ are reasonable, but can be further refined. Meanwhile, a new equation can be proposed to predict $\varepsilon_{uT}$ of austenitic and duplex stainless steels, since Eq. (9) originally proposed by Wang et al.[15] assumes a constant $\varepsilon_{uT}$ up to 1000 °C.

Based on regression analysis, Eq. (13) is proposed to predict $f_{yT}$ of austenitic and duplex stainless steels, whereas Eq. (14) is proposed to predict the corresponding ultimate strain $\varepsilon_{uT}$.

$$\frac{f_{yT}}{f_y} = \begin{cases} 1 & T \le 500\ ℃ \\ 1 - 4 \times 10^{-4}(T - 500) & 500\ ℃ < T \le 1200\ ℃ \end{cases} \quad \text{for austenitic and duplex alloys} \tag{13}$$

$$\frac{\varepsilon_{uT}}{\varepsilon_u} = \begin{cases} 1 & T \le 800\ ℃ \\ 1 + 6.5 \times 10^{-4}(T - 800) & 800\ ℃ < T \le 1200\ ℃ \end{cases} \quad \text{for austenitic and duplex alloys} \tag{14}$$

For ferritic stainless steel, Eqs. (15) and (16) are proposed to predict $f_{yT}$ and $\varepsilon_{uT}$, respectively:

$$\frac{f_{yT}}{f_y} = \begin{cases} 1 & T \le 500℃ \\ 1 - 9 \times 10^{-4}(T - 500) & 500\ ℃ < T \le 800\ ℃ \\ 0.73 + 6.75 \times 10^{-4}(T - 800) & 800\ ℃ < T \le 1200\ ℃ \end{cases} \quad \text{for ferritic alloy} \tag{15}$$

$$\frac{\varepsilon_{uT}}{\varepsilon_u} = \begin{cases} 1 & T \le 800\ ℃ \\ 1 - 4.4 \times 10^{-3}(T - 800) & 800\ ℃ < T \le 1000\ ℃ \\ 0.12 & 1000\ ℃ < T \le 1200\ ℃ \end{cases} \quad \text{for ferritic alloy} \tag{16}$$

Due to the significant variation in the measured $\varepsilon_{uT}$ of austenitic and duplex stainless steels, the coefficient of determination $R^2$ is only 0.32 for the regression, indicating relatively low accuracy of Eq. (14). Reasonable regression accuracy is obtained for $\varepsilon_{uT}$ of ferritic stainless steel. The prediction accuracy of $f_{yT}$ is also reasonable for all grades, but the $R^2$–values have been affected by neglecting the minor strength increase of duplex and ferrtic stainless steels in the temperature range 300–500 °C. In general, the prediction of $f_{yT}$ based on Eq. (13) or Eq. (15) is on the safe side.

### 5.3 Strain hardening exponent $n_T$

Figs. 17–19 show the relationship between $n_T/n$ and temperature $T$ for the three types of stainless steels, which demonstrate different trends as $T$ increases. It should be noted that the measured $n_T$ shows significant variation partly because of the variation in measurements of $E_{sT}$, as explained earlier. In general, $n_T$ remains unchanged when the temperature is less than 500 °C. Wang et al.[15] suggested a constant $n_T$ up to 1000 °C for austenitic stainless steel. But the current test data of austenitic stainless steel suggest an increasing trend for $n_T$ when $T$ increases from 500 to 800 °C before stabilisation (Fig. 17). Further tests should be performed to verify the findings. $n_T$ of the duplex stainless steel shows a clear decreasing trend when $T$ is greater than 500 °C (Fig. 18). In contrast, $n_T$ of the ferritic stainless steel increases sharply from 500 °C, and reaches its peak at 800 °C, followed by a sudden drop to around 50% that of the unheated material at 1200 °C (Fig. 19). This sudden drop in $n_T$ coincides with the abrupt reduction in ductility at 800 °C shown in Fig. 16.

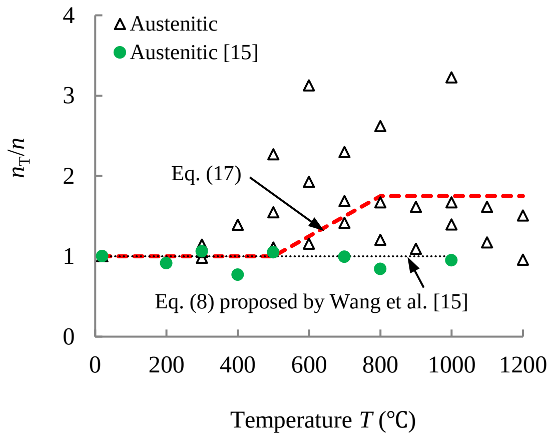


**Fig. 17. $n_T/n$ versus $T$ for austenitic stainless steel.**

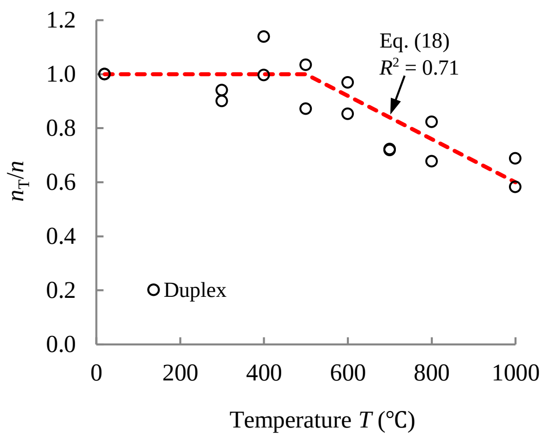


**Fig. 18. $n_T/n$ versus $T$ for duplex stainless steel.**

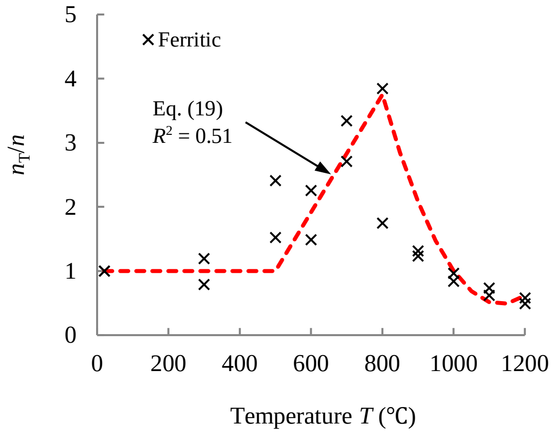


**Fig. 19. $n_T/n$ versus $T$ for ferritic stainless steel.**

Based on regression analysis, Eqs. (17)–(19) are proposed to predict $n_T$ for austenitic, duplex and ferritic stainless steels, respectively. It seems the prediction accuracy for duplex and ferritic stainless steels is better than that for austenitic stainless steel.

$$\frac{n_T}{n} = \begin{cases} 1 & T \le 500\ ^\circ\mathrm{C} \\ 1 + 2.5 \times 10^{-3}(T - 500) & 500\ ^\circ\mathrm{C} < T \le 800\ ^\circ\mathrm{C} \\ 1.75 & 800\ ^\circ\mathrm{C} < T \le 1200\ ^\circ\mathrm{C} \end{cases} \quad \text{for austenitic alloy} \tag{17}$$

$$\frac{n_T}{n} = \begin{cases} 1 & T \le 500\ ^\circ\mathrm{C} \\ 1 - 8 \times 10^{-4}(T - 500) & 500\ ^\circ\mathrm{C} < T \le 1000\ ^\circ\mathrm{C} \end{cases} \quad \text{for duplex alloy} \tag{18}$$

$$\frac{n_T}{n} = \begin{cases} 1 & T \le 500\ ^\circ\mathrm{C} \\ 1 + 9.17 \times 10^{-3}(T - 500) & 500\ ^\circ\mathrm{C} < T \le 800\ ^\circ\mathrm{C} \\ 3.75 - 1.96 \times 10^{-2}(T - 800) + 2.94 \times 10^{-5}(T - 800)^2 & 800\ ^\circ\mathrm{C} < T \le 1200\ ^\circ\mathrm{C} \end{cases} \quad \text{for ferritic alloy} \tag{19}$$

## 5.4 Stress $f_{fT}$, strain $\varepsilon_{fT}$ and modulus $E_{fT}$ at the fracture point

At the fracture point, three parameters—stress $f_{fT}$, strain $\varepsilon_{fT}$ and modulus $E_{fT}$—can be derived from the $\sigma$–$\varepsilon$ curves. It is found that $f_{fT}/f_{yT}$ is proportional to the ratio of $f_{uT}/f_{yT}$, as shown in Fig. 20. Meanwhile, a bilinear relationship is found between $\varepsilon_{fT}$ and $\varepsilon_{uT}$, as shown in Fig. 21. It is observed that the shape of a $\sigma$–$\varepsilon$ curve in the necking stage has not been obviously affected by heat exposure. To confirm this, a total of 27 room temperature curves were collected from 10 references[8,12,17,25–31], and the corresponding data are also plotted in Figs. 20 and 21. Clearly, the $f_{fT}/f_{yT}$–$f_{uT}/f_{yT}$ relation or $\varepsilon_{fT}$–$\varepsilon_{uT}$ relation is applicable to both room temperature stainless steel and that after exposure to elevated temperature. Therefore, the two types of test data are combined together for the purpose of regression analysis.

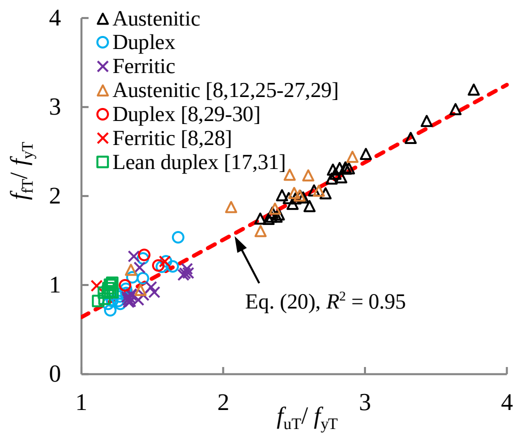


**Fig. 20. $f_{fT}/f_{yT}$ versus $f_{uT}/f_{yT}$ for all grades.**

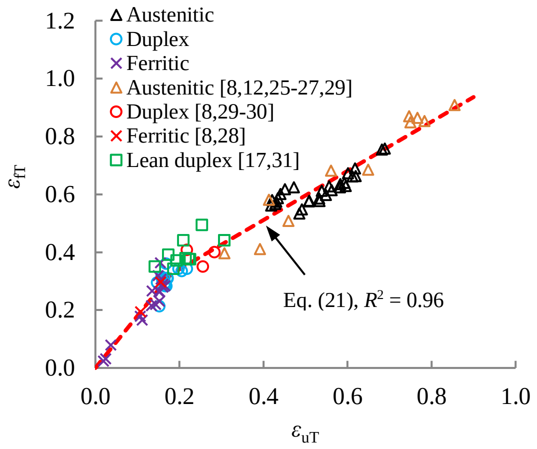


**Fig. 21. $\varepsilon_{fT}$ versus $\varepsilon_{uT}$ for all grades.**

Based on regression analysis, Eqs. (20) and (21) are proposed to predict $f_{fT}$ and $\varepsilon_{fT}$, respectively. The coefficients of determination $R^2$ are 0.95 and 0.96 for the regressions of $f_{fT}$ and $\varepsilon_{fT}$, respectively. As shown in Figs. 20 and 21, the predicted values from the equations have very good correlation with the test data.

As shown in Fig. 22, the ratio of $E_{fT}/E_{sT}$ varies from 0.021 to 0.081 for the combined test data of all stainless steel grades. Because of the significant variation, no clear trend can be found for $E_{fT}$ as temperature increases. Therefore, Eq. (22) is suggested to predict $E_{fT}$, where the average value of $0.04E_{sT}$ is adopted.

$$\frac{f_{fT}}{f_{yT}} = 0.64 + 0.87\left(\frac{f_{uT}}{f_{yT}} - 1\right) \qquad 1 < \frac{f_{uT}}{f_{yT}} \le 4 \tag{20}$$

$$\varepsilon_{fT} = \begin{cases} 1.8\varepsilon_{uT} & \varepsilon_{uT} \le 0.18 \\ 0.324 + 0.85(\varepsilon_{uT} - 0.18) & \varepsilon_{uT} > 0.18 \end{cases} \tag{21}$$

$$\frac{E_{fT}}{E_{sT}} = 0.04 \tag{22}$$

## 5.5 Effects of variations in $E_{sT}$, $n_T$ and $E_{fT}$ on prediction accuracy

Considerable variations in $E_{sT}$, $n_T$ and $E_{fT}$ can be found in Figs. 11, 17 and 22, respectively; the variations may affect the prediction accuracy of post-fire $\sigma$–$\varepsilon$ curves. As shown in Fig. 11, $E_{sT}$ ranges from $0.82E_s$ to $1.20E_s$ at $T$ = 1000 °C and the corresponding variation from $E_s$ is between −18% and +20%. $n_T$ ranges from $0.77n$ to $3.23n$ for austenitic stainless steel, as demonstrated in Fig. 17. The maximum variation in $n_T$ appears at $T$ = 1000 °C, where the predicted $n_T$–value from Eq. (17) is $1.75n$. Accordingly, the variation from the predicted $n_T$ at this temperature is between –56% and +85%. From Fig. 22, it can be found that $E_{fT}$ ranges from $0.021E_{sT}$ to $0.081\ E_{sT}$. Compared with the suggested $E_{fT}$–value of $0.04E_{sT}$, the corresponding variation ranges from –47% to +103%.

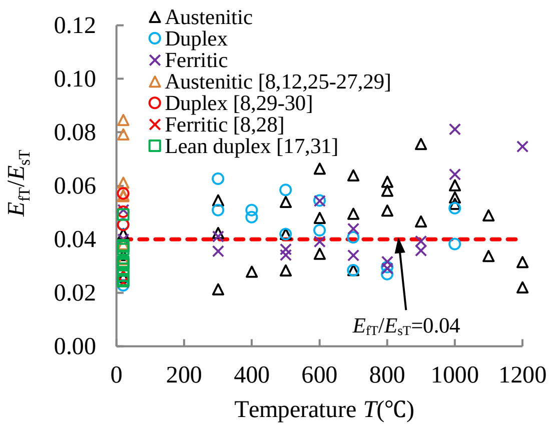


**Fig. 22. $E_{fT}/E_{sT}$ versus $T$ for all grades.**

The variations in $E_{sT}$, $n_T$ and $E_{fT}$ on the prediction accuracy of post-fire $\sigma$–$\varepsilon$ curves are evaluated by adopting the upper limit, mean (predicted) value and lower limit of each parameter; the obtained curves based on the proposed model are shown in Figs. 23–25, respectively. The evaluation is conducted on the austenitic grade 1.4307 stainless steel extracted from a SHS ($E_s$ = 194300 MPa, $f_y$ = 274.9 MPa, $f_u$ = 664.0 MPa, $n$ = 10.1 and $\varepsilon_u$ = 0.485); the temperature is taken as 1000 °C. In Figs. 23 and 24, $\varepsilon_p$ is the plastic strain.

The variation in $E_{sT}$ mainly affects Stage 1 (before reaching $f_{yT}$) of the $\sigma$–$\varepsilon$ curve (Figs. 23), whereas some influence of $n_T$ can be observed for both Stage 1 and Stage 2 (Figs. 24). In contrast, the variation in $E_{fT}$ only affects the last (necking) stage of the curve (Fig. 25), leading to a maximum stress variation at a strain $\varepsilon$ of 0.62 for this example. Based on this observation, the changes in stresses $f_{0.05p}$, $f_{yT}$ and $f_{1\%}$ corresponding to the variation of $E_{sT}$ are calculated, where $f_{0.05p}$ is the 0.05% proof stress, $f_{yT}$ is the 0.2% proof stress, and $f_{1\%}$ is the stress at $\varepsilon = 1\%$. Since the variation of $n_T$ does not affect the yield stress $f_{yT}$, the stresses of $f_{0.05p}$, $f_{1\%}$ and $f_{2\%}$ are determined, where $f_{2\%}$ is the stress at $\varepsilon = 2\%$. To evaluate the influence of the variation of $E_{fT}$, only $f_{62\%}$ is determined, where $f_{62\%}$ is the stress at $\varepsilon = 0.62$. The maximum percentage variations in these selected stresses are summarised in Table 5 due to the given percentage variations in the three input parameters ($E_{sT}$, $n_T$ and $E_{fT}$). As can be seen in Table 5, a decrease in $E_{sT}$ of 18% leads to a maximum decrease in $f_{0.05p}$ of only 3.1%; the influence of variation in $E_{sT}$ on $f_{yT}$ and $f_{1\%}$ is less significant (from –1% to 0.6%). A decrease in $n_T$ of 56% results in a decrease in $f_{0.05p}$ of 9.0%. The maximum changes in $f_{1\%}$ and $f_{2\%}$, however, are just around 5%, which is moderate. The maximum change in $f_{62\%}$ is also around 5% because of the variation in $E_{fT}$. Although there are considerable variations in $E_{sT}$, $n_T$ and $E_{fT}$, it seems the corresponding influence on the predicted $\sigma$–$\varepsilon$ curves is not significant (Figs. 23–25).

**Table 5. Effects of variations in $E_{sT}$, $n_T$ and $E_{fT}$ on predicted stress.**

| Variation | $E_{sT}$ | | | | | $n_T$ | | | | | $E_{fT}$ | | |
|---|---|---|---|---|---|---|---|---|---|---|---|---|---|
| | Adopted $E_{sT}$ (MPa) | Change In $E_{sT}$ (%) | Change in $f_{0.05p}$ (%) | Change in $f_{yT}$ (%) | Change in $f_{1\%}$ (%) | Adopted $n_T$ | Change in $n_T$ (%) | Change in $f_{0.05p}$ (%) | Change in $f_{1\%}$ (%) | Change in $f_{2\%}$ (%) | Adopted $E_{fT}$ (MPa) | Change in $E_{fT}$ (%) | Change in $f_{62\%}$ (%) |
| Upper limit | 233200 | +20 | +1.8 | +0.6 | +0.3 | 32.7 | +85 | +4.1 | –4.4 | –5.4 | 15800 | +103 | +5.2 |
| Mean | 194300 | 0 | 0 | 0 | 0 | 17.7 | 0 | 0 | 0 | 0 | 7800 | 0 | 0 |
| Lower limit | 159300 | –18 | –3.1 | –1.0 | –0.4 | 7.8 | –56 | –9.0 | +5.0 | +5.2 | 4100 | –47 | –5.1 |

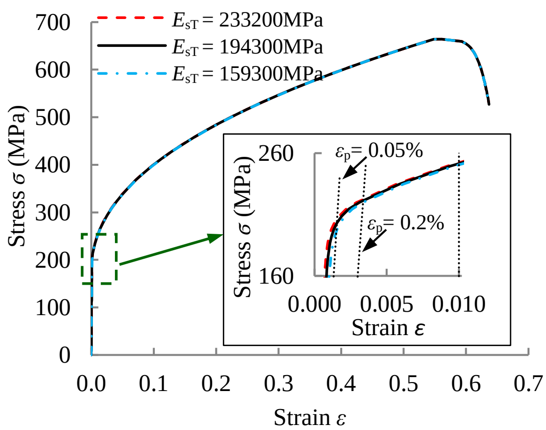


**Fig. 23. Effect of $E_{sT}$ on stress–strain curve.**

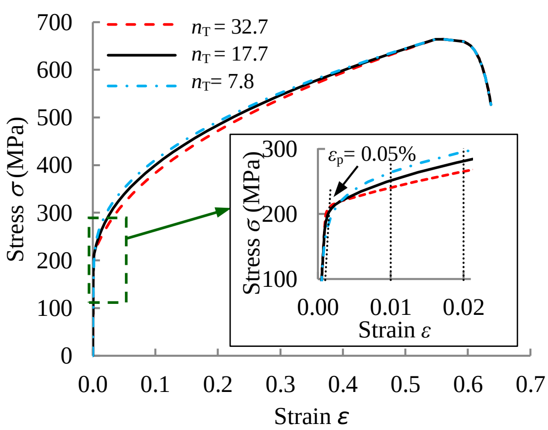


**Fig. 24. Effect of $n_T$ on stress–strain curve.**

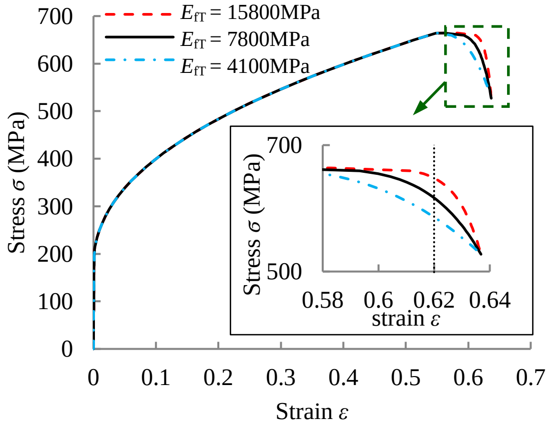

**Fig. 25. Effect of $E_{fT}$ on stress–strain curve.**

# 6 Validation of the Revised Stress–strain Model

## 6.1 Summary of equations

The revised $\sigma$–$\varepsilon$ model is expressed by Eq. (10), which can be used to predict the post-fire mechanical behaviour of austenitic, duplex and ferritic alloys. To use this model, a total of 8 key parameters need to be determined, including $E_{sT}$, $f_{yT}$, $f_{uT}$, $n_T$, $\varepsilon_{uT}$, $f_{fT}$, $\varepsilon_{fT}$ and $E_{fT}$. The corresponding expressions for these parameters are summarised in Table 6. By using Eq. (10) in combination with the equations presented in Table 6, the post-fire $\sigma$–$\varepsilon$ curve at a given temperature $T$ can be determined based on the five room temperature parameters of stainless steel, i.e., $E_s$, $f_y$, $f_u$, $n$, and $\varepsilon_u$.

**Table 6. Summary of expressions for $E_{sT}$, $f_{yT}$, $f_{uT}$, $n_T$, $\varepsilon_{uT}$, $f_{fT}$, $\varepsilon_{fT}$ and $E_{fT}$.**

| Parameter | Expression | Steel type | Equation number |
|---|---|---|---|
| $E_{sT}$ | $\frac{E_{sT}}{E_s} = 1$ | All grades | (6) |
| $f_{yT}$ | $\frac{f_{yT}}{f_y} = \begin{cases} 1 & T \le 500\ ℃ \\ 1 - 4\times10^{-4}(T-500) & 500\ ℃ < T \le 1200\ ℃ \end{cases}$ | Austenitic & duplex | (13) |
| | $\frac{f_{yT}}{f_y} = \begin{cases} 1 & T \le 500\ ℃ \\ 1 - 9\times10^{-4}(T-500) & 500\ ℃ < T \le 800\ ℃ \\ 0.73 + 6.75\times10^{-4}(T-800) & 800\ ℃ < T \le 1200\ ℃ \end{cases}$ | Ferritic | (15) |
| $f_{uT}$ | $\frac{f_{uT}}{f_u} = 1$ | All grades | (7) |
| $n_T$ | $\frac{n_T}{n} = \begin{cases} 1 & T \le 500\ ℃ \\ 1 + 2.5\times10^{-3}(T-500) & 500\ ℃ < T \le 800\ ℃ \\ 1.75 & 800\ ℃ < T \le 1200\ ℃ \end{cases}$ | Austenitic | (17) |
| | $\frac{n_T}{n} = \begin{cases} 1 & T \le 500\ ℃ \\ 1 - 8\times10^{-4}(T-500) & 500\ ℃ < T \le 1000\ ℃ \end{cases}$ | Duplex | (18) |
| | $\frac{n_T}{n} = \begin{cases} 1 & T \le 500\ ℃ \\ 1 + 9.17\times10^{-3}(T-500) & 500\ ℃ < T \le 800\ ℃ \\ 3.75 - 1.96\times10^{-2}(T-800) + 2.94\times10^{-5}(T-800)^2 & 800\ ℃ < T \le 1200\ ℃ \end{cases}$ | Ferritic | (19) |
| $\varepsilon_{uT}$ | $\frac{\varepsilon_{uT}}{\varepsilon_u} = \begin{cases} 1 & T \le 800\ ℃ \\ 1 + 6.5\times10^{-4}(T-800) & 800\ ℃ < T \le 1200\ ℃ \end{cases}$ | Austenitic & duplex | (14) |
| | $\frac{\varepsilon_{uT}}{\varepsilon_u} = \begin{cases} 1 & T \le 800\ ℃ \\ 1 - 4.4\times10^{-3}(T-800) & 800\ ℃ < T \le 1000\ ℃ \\ 0.12 & 1000\ ℃ < T \le 1200\ ℃ \end{cases}$ | Ferritic | (16) |
| $f_{fT}$ | $\frac{f_{fT}}{f_{yT}} = 0.64 + 0.87\left(\frac{f_{uT}}{f_{yT}} - 1\right) \quad 1 < \frac{f_{uT}}{f_{yT}} \le 4$ | All grades | (20) |
| $\varepsilon_{fT}$ | $\varepsilon_{fT} = \begin{cases} 1.8\varepsilon_{uT} & \varepsilon_{uT} \le 0.18 \\ 0.324 + 0.85(\varepsilon_{uT} - 0.18) & \varepsilon_{uT} > 0.18 \end{cases}$ | All grades | (21) |
| $E_{fT}$ | $\frac{E_{fT}}{E_{sT}} = 0.04$ | All grades | (22) |

## 6.2 Comparison between predicted and measured stress–strain curves

In Section 5, the test data have been used to propose equations for key parameters in the $\sigma$–$\varepsilon$ model of stainless steel after exposure to elevated temperatures. Since the prediction accuracy of these equations has been rigorously verified, it is expected that good agreement should be achieved between the predicted and measured $\sigma$–$\varepsilon$ curves. This is confirmed by the comparisons shown in Fig. 26 between the predictions and typical measured $\sigma$–$\varepsilon$ curves of the three types of stainless steel. It should be noted that the measured $\sigma$–$\varepsilon$ curve of sheet material often demonstrates slightly stronger strain-hardening behaviour than the predicted curve. However, the difference is not very significant and the prediction is generally on the safe side.

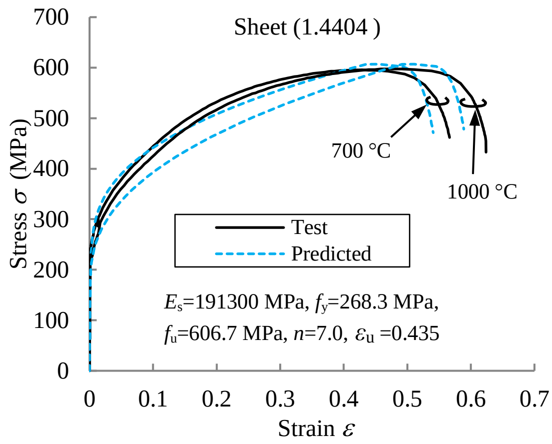


(a) Austenitic sheet (1.4404)

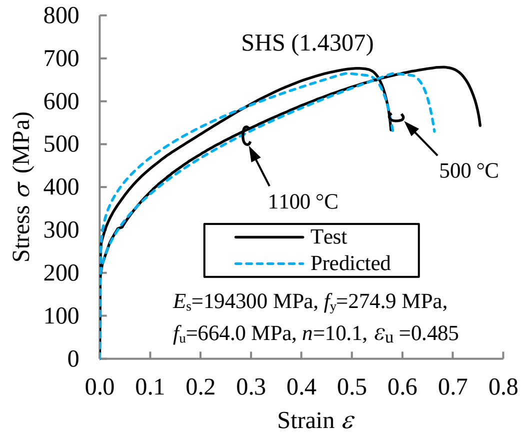


(b) Austenitic SHS flat (1.4307)

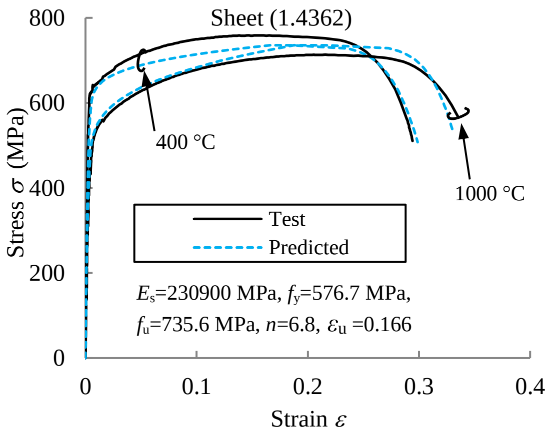


(c) Duplex sheet (1.4362)

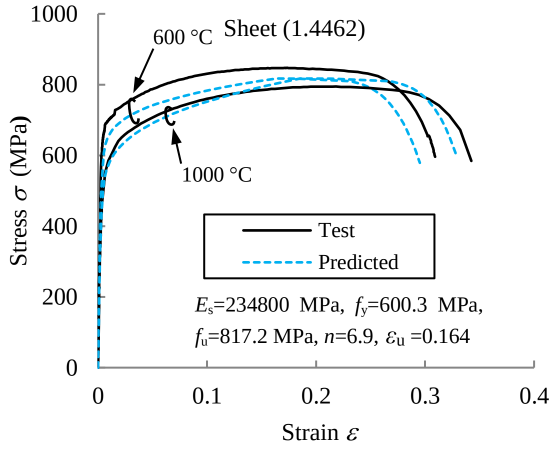


(d) Duplex sheet (1.4462)

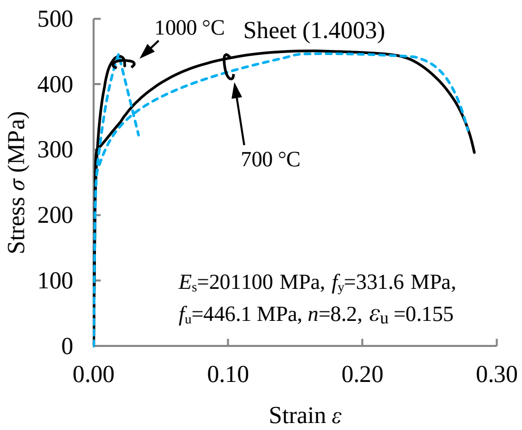


(e) Ferritic sheet (1.4003)

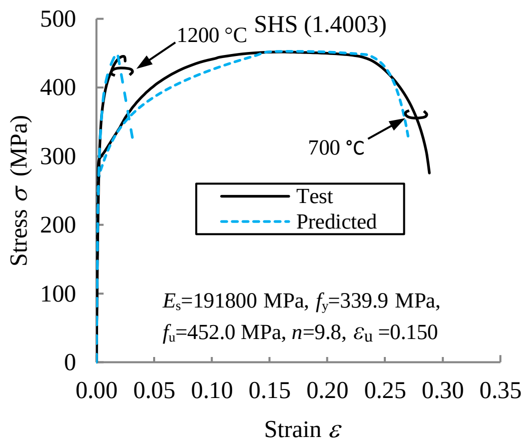


(f) Ferritic SHS flat (1.4003)

**Fig. 26. Comparison between predicted and measured stress–strain curves.**

As mentioned earlier, five room temperature parameters of stainless steel—$E_s$, $f_y$, $f_u$, $n$ and $\varepsilon_u$—are required to generate the full-range $\sigma$–$\varepsilon$ curve of steel after exposure to elevated temperatures. It is possible to eliminate the use of $f_u$ and $\varepsilon_u$, since a number of equations are available in the literature to statistically predict $f_u$ and $\varepsilon_u$ based on $f_y$ and $E_s$[4,7,8]. For example, Eqs. (23) and (24) were proposed by Rasmussen[4] to predict $f_u$ and $\varepsilon_u$, respectively, for austenitic and duplex alloys. On the other hand, Tao and Rasmussen[7] proposed corresponding Eqs. (25) and (26) for ferritic alloy. If these equations are used, only three basic parameters ($E_s$, $f_y$ and $n$) are required to predict the full-range $\sigma$–$\varepsilon$ curve at a given $T$.

$$\frac{f_y}{f_u} = 0.2 + 185\frac{f_y}{E_s} \quad \text{for austenitic and duplex alloys} \tag{23}$$

$$\varepsilon_u = 1 - \frac{f_y}{f_u} \quad \text{for austenitic and duplex alloys} \tag{24}$$

$$\frac{f_y}{f_u} = \begin{cases} 0.104 + 360\frac{f_y}{E_s} & 0.00125 \le \frac{f_y}{E_s} \le 0.00235 \\ 0.95 & 0.00235 < \frac{f_y}{E_s} \le 0.00275 \end{cases} \quad \text{for ferritic alloy} \tag{25}$$

$$\varepsilon_u = 0.2 - 0.2\left(\frac{f_y}{f_u}\right)^{5.5} \quad \text{for ferritic alloy} \tag{26}$$

It should be noted, however, Eqs. (23–26) can give significant prediction errors. According to Rasmussen[4], Eq. (23) can have prediction errors of more than 20% for $f_u$, whereas the prediction errors of $\varepsilon_u$ using Eq. (24) can be more than 40%. This is also confirmed by the current test results. For example, the predicted $f_u$ of the austenitic 1.4307 from Eq. (23) is underestimated by 18.9%, although Eq. (24) only slightly underestimates $\varepsilon_u$ by 4.8%. Accordingly, the post-fire strength of this material at a large deformation is underestimated (Fig. 27a) when the $\sigma$–$\varepsilon$ curve is predicted using the calculated $f_u$ from Eq. (23) rather than the measured $f_u$. On the other hand, Eqs. (23) and (24) overestimate the ultimate strength and corresponding strain of the two types of duplex stainless steel. For instance, $f_u$ and $\varepsilon_u$ are overestimated by 9.2% and 99.4%, respectively, for the duplex grade 1.4462. Therefore, the deformation capacity of this material is significantly overestimated (Fig. 27b) if the calculated $f_u$ and $\varepsilon_u$ are used in predicting the post-fire $\sigma$–$\varepsilon$ curve. Instead, the prediction accuracy of the post-fire $\sigma$–$\varepsilon$ curve can be significantly improved if based on five parameters ($E_s$, $f_y$, $f_u$, $n$ and $\varepsilon_u$) rather than three parameters ($E_s$, $f_y$ and $n$) in these cases. This can be clearly seen from the comparison shown in Fig. 27. Meanwhile, it should be noted that reasonable good predictions of the post-fire $\sigma$–$\varepsilon$ curves have also been obtained for the austenitic grade 1.4404 and ferritic grade 1.4003 materials by using the three parameters of $E_s$, $f_y$ and $n$. Because of the variation in prediction accuracy, tensile tests on room temperature stainless steel are recommended to measure $E_s$, $f_y$, $f_u$, $n$ and $\varepsilon_u$ if high accuracy is required in predicting the full-range stress–strain curves of stainless steel after exposure to elevated temperatures.

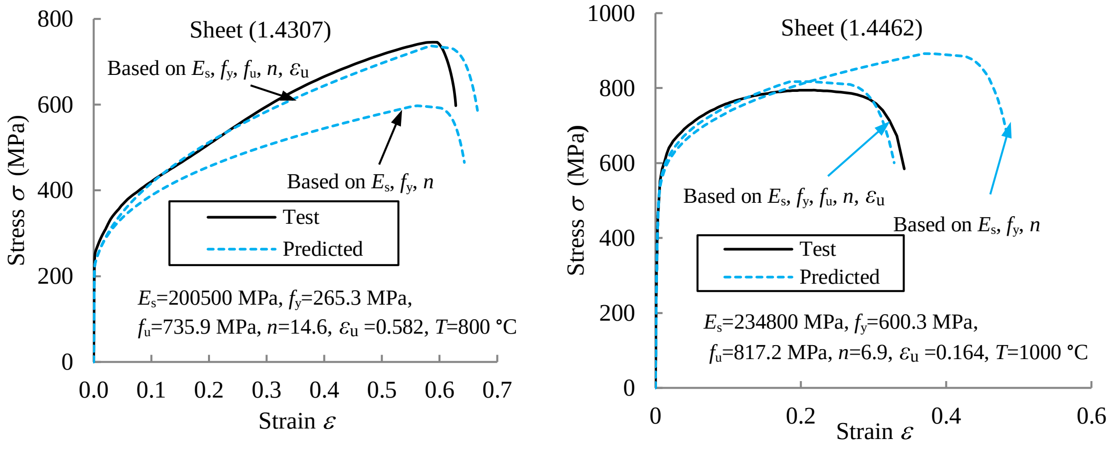


(a) Austenitic sheet (1.4307) (b) Duplex sheet (1.4462)

**Fig. 27. Comparison of predicted stress–strain curves obtained from different basic parameters.**

## 7 Comparison of Post-fire Properties Between Different Types of Steel

In Sections 3 and 5, the post-fire properties of three types of stainless steel have been investigated and compared with one another. Useful information can be obtained if the post-fire properties of stainless steel are further compared with those of mild steel and low-carbon high-strength steel. Test data of three types of sheet materials (austenitic grade 1.4307, duplex grade 1.4362 and ferritic grade 1.4003) reported in Section 3 are compared with test data reported by Lee et al.[32] and Qiang et al.[33] for typical mild steel ($f_y$ = 358.5 MPa) and high-strength steel ($f_y$ = 789.0 MPa).

Figs. 28–30 compare the effects of temperature on the normalised yield stress ($f_{yT}/f_y$), ultimate strength ($f_{uT}/f_u$) and ultimate strain ($\varepsilon_{uT}/\varepsilon_u$) of different types of steel, respectively. When the temperature is 500 °C or lower, no obvious change in behaviour can be found for different types of steel if the embrittlement effect of the duplex and ferritic alloys in the temperature range of 280–500 °C is ignored. It should be noted that, however, some researchers have reported strength deterioration of high-strength steel as early as 300 °C[19]. Beyond 600 °C, strength deterioration of all types of steel becomes obvious, but difference in behaviour between different types of steel can be observed. As shown in Fig. 28, the retention of yield stress is highest for austenitic alloy at 800 °C, followed by mild steel, duplex alloy and ferritic alloy. The high-strength steel has the largest strength loss at the same temperature. Generally, increased strength loss is expected when the temperature increases further. But a recovery in yield stress is observed for ferritic alloy beyond 800 °C due to the embrittlement. As illustrated in Fig. 29, the influence of temperature on the ultimate strength is less significant than that on the yield stress. In general, very minor decrease in ultimate strength is observed for all types of steel except for the significant decrease in $f_{uT}$ for high strength steel beyond 600 °C. The influence of temperature on the ultimate strain $\varepsilon_{uT}$ is also minor for austenitic alloy, duplex alloy and mild steel. But significant reduction in $\varepsilon_{uT}$ is observed for ferritic alloy beyond 800 °C. In contrast, the high-strength steel demonstrates significant recovery in ultimate strain due to the diminishing effect of quenching and tempering[34].

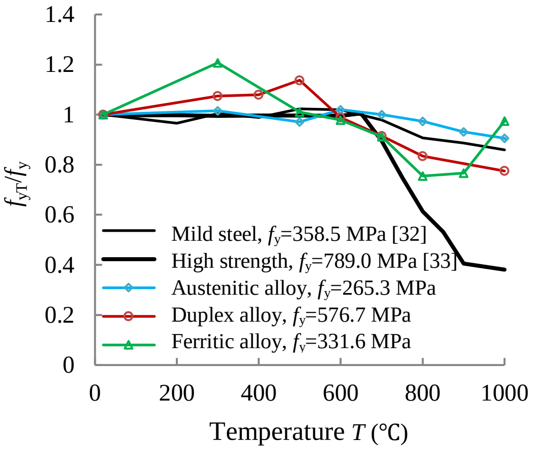


**Fig. 28. Effect of $T$ on $f_{yT}/f_y$ of different types of steel.**

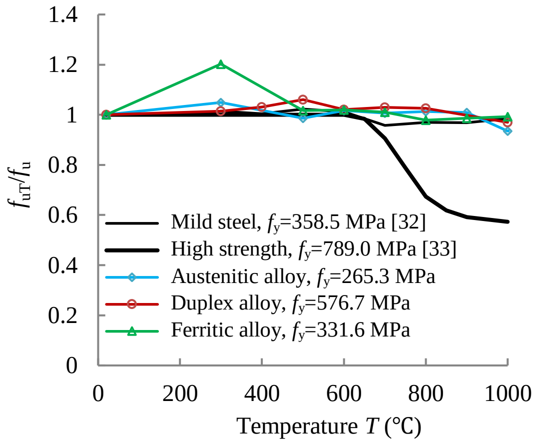


**Fig. 29. Effect of $T$ on $f_{uT}/f_u$ of different types of steel.**

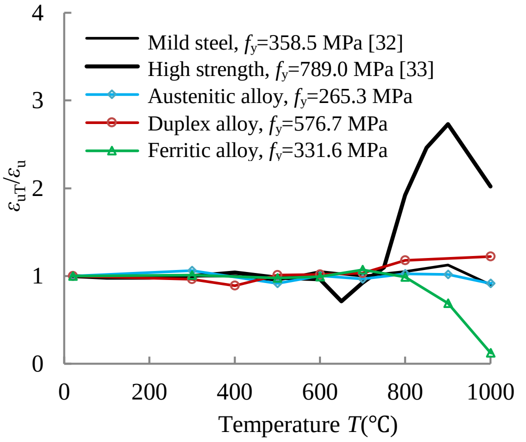


**Fig. 30. Effect of $T$ on $\varepsilon_{uT}/\varepsilon_u$ of different types of steel.**

## 8 Conclusions

Experimental studies have been conducted to investigate the mechanical properties of austenitic, duplex and ferritic stainless steels after exposure to elevated temperatures up to 1200 °C. The following conclusions can be drawn within the scope of this study:

1. When the temperature $T$ is 500 °C or lower, its influence on the stress–strain ($\sigma$–$\varepsilon$) curve is negligible for all stainless steel grades. But strength deterioration becomes obvious when the temperature reaches 600 °C or higher.

2. Different types of stainless steel behave differently after fire exposure. For austenitic and duplex alloys, the ductility increases slightly beyond 800 °C. However, the ductility of ferritic stainless steel reduces significantly beyond this temperature, whereas the yield stress increases. Cold forming effect has been found for austenitic stainless steel extracted from the flat parts of square hollow sections, and this effect diminishes at 900 °C and above. However, no obvious cold forming effect is found in ferritic stainless steel flat coupons.

3. Based on regression analysis, suitable modifications have been made to an existing $\sigma$–$\varepsilon$ model proposed by the authors for austenitic stainless steel in earlier research. At a given temperature, the post-fire $\sigma$–$\varepsilon$ curve can be determined based on the five room temperature parameters of stainless steel—elastic modulus $E_s$, yield stress $f_y$, ultimate strength $f_u$, strain hardening exponent $n$ and ultimate strain $\varepsilon_u$. The modified model with a post-peak stage is suitable for evaluating the post-fire behaviour of all three types of stainless steel (i.e., austenitic, duplex and ferritic alloys). The accuracy of the model has been validated by comparing with the test results.

4. The post-fire properties of stainless steel have been compared with those of mild steel and low-carbon high-strength steel based on test data. At a low temperature (≤500 °C), the behaviour difference between different types of steel is not significant. When the temperature reaches 600 °C or above, strength deterioration becomes obvious for all types of steel. In general, austenitic alloy has the best performance, followed by mild steel and duplex alloy. Ferritic alloy has higher strength retention than high-strength steel, but the brittle failure of ferritic alloy beyond 800 °C is a concern. Further research is required on the post-fire properties of ferritic stainless steel.

## Acknowledgments

This work is supported by the Australian Research Council Discovery Project (Grant No: DP120100971). It is also partly supported by Project of Science and Technology of Shandong Colleges and Universities (Project No: J14LG52), and Research Supporting Project of Shandong Polytechnic (Project No: KY-W201403). The financial support is highly appreciated. The authors would also like to express special thanks to Mr. Laith Almoaiel for his assistance in the experiments.

## References

[1] L. Gardner, The use of stainless steel in structures, Prog. Struct. Engng. Mater. 7 (2005) 45–55.

[2] EN 10088-5, Stainless steels, Technical delivery conditions for bars, rods, wire, sections and bright products of corrosion resisting steels for construction purposes, Brussels, European Committee for Standardization, 2009.

[3] E. Mirambell, E. Real, On the calculation of deflections in structural stainless steel beams: An experimental and numerical investigation, J. Constr. Steel Res. 54 (1) (2005) 109–133.

[4] K.J.R. Rasmussen, Full-range stress-strain curves for stainless steel alloys, J. Constr. Steel Res. 59 (1) (2003) 47–61.

[5] L. Gardner, M. Ashraf, Structural design for non-linear metallic materials, Eng. Stru. 28 (6) (2006) 926–934.

[6] W.M. Quach, J.G. Teng, K.F. Chung, Three-stage full-range stress–strain model for stainless steels, J. Struct. Eng. 134 (9) (2008) 1518–1527.

[7] Z. Tao, K.J.R. Rasmussen, Stress-strain model for ferritic stainless steels, J. Mater. Civ. Eng. 28 (2) (2016) 1−5.

[8] I. Arrayago, E. Real, L. Gardner. Description of stress-strain curves for stainless steel alloys, Mater. Des. 87 (2015) 540–552.

[9] P. Mäkeläinen, J. Outinen, Mechanical properties of an austenitic stainless steel at elevated temperatures, J. Constr. Steel Res. 46 (1-3) (1998) 455.

[10] J. Chen, B. Young, Stress-strain curves for stainless steel at elevated temperatures, Eng. Struct. 28 (2) (2006) 229–239.

[11] L. Gardner, A. Insausti, K.T. Ng, M. Ashraf, Elevated temperature material properties of stainless steel alloys, J. Constr. Steel Res. 66 (5) (2010) 634–647.

[12] L. Gardner, Y. Bu, P. Francis, N.R. Baddoo, K.A. Cashell, F. McCann, Elevated temperature material properties of stainless steel reinforcing bar, Constr. Build. Mater. 114 (2016) 977−997.

[13] EN 1993–1-2:2005, Design of steel structures–Part 1-2: General rules-structural fire design, European Committee for Standardization, Brussels, 2005.

[14] R. Felicetti, P.G. Gambarova, A. Meda, Residual behavior of steel rebars and R/C sections after a fire, Constr. Build. Mater. 23 (12) (2009) 3546–3555.

[15] X.Q. Wang, Z. Tao, T.Y. Song, L.H. Han, Stress-strain model of austenitic stainless steel after exposure to elevated temperatures, J. Constr. Steel Res. 99 (2014) 129–139.

[16] Standards Australia, Metallic materials-tensile testing at ambient temperature, AS 1391−2007, Sydney, Australia, 2007.

[17] Y. Huang, B. Young, The art of coupon tests, J. Constr. Steel Res. 96 (2014) 159–175.

[18] EN 1993-1-4:2006, Design of steel structures, Part 1−4: General rules−supplementary rules for stainless steel, European Committee for Standardization, Brussels, 2006.

[19] Z. Tao, X.Q. Wang, B. Uy, Stress-strain curves of structural and reinforcing steels after exposure to elevated temperatures, J. Mater. Civ. Eng. 25 (9) (2013) 1306–1316.

[20] J.K. Sahu, U. Krupp, R.N. Ghosh, H.J. Christ, Effect of 475 °C embrittlement on the mechanical properties of duplex stainless steel, Mater. Sci. Eng. A 508(1-8) (2009) 1−14.

[21] A.C.T.M. Van Zwieten, Some considerations on the toughness properties of ferritic stainless steels–A brief Review, Int. J. Pres. Ves. & Piping 56 (1993) 1–31.

[22] F.A. Alhegagi, 475°C embrittlement in stainless steels, Int. J. Sci. Eng. Res. 6 (9) (2015) 145–154.

[23] M.L. Greef, T.M. Du, Sensitisation of two 11–12 % chromium type EN 1.4003 ferritic stainless steels during continuous cooling after welding, Weld. World 50 (7-8) (2006)18–27.

[24] C. Grobler, Weldability studies on 12% and 14% chromium steels, PhD dissertation, University of Pretoria, 1987, South Africa.

[25] J. Fan, T. Fu, Toughened austenitic stainless steel by surface severe plastic deformation, Mater. Sci. Eng. A 552 (2012) 359–363.

[26] W.M. Quach, P. Qiu, Strength and ductility of corner materials in cold-formed stainless steel sections, Thin-walled Struct. 83 (2014) 28–42.

[27] M. Okayasu, S. Tomida, Phase transformation system of austenitic stainless steels obtained by permanent compressive strain, Mater. Sci. Eng. A 684 (2017) 712–725.

[28] M. Bock, I. Arrayago, E. Real, Experiments on cold-formed ferritic stainless steel slender sections, J. Constr. Steel Res. 109 (2015) 13–23.

[29] L. Yang, M.H. Zhao, T.M. Chan, F. Shang, D.C. Xu, Flexural buckling of welded austenitic and duplex stainless steel I-section columns, J. Constr. Steel Res. 122 (2016) 339–353.

[30] B. Young, W.M. Lui, Tests of cold-formed high strength stainless steel compression members, Thin-Walled Struct. 44 (2) (2006) 224–234.

[31] Y. Huang, B. Young. Material properties of cold-formed lean duplex stainless steel sections, Thin-Walled Struct. 54 (2012) 72–81.

[32] J. Lee, M.D. Engelhardt, Post-fire mechanical properties of ASTM A992 steel, Proceedings of the 6th International Symposium on Steel Structures, Seoul, Korea, 1004–1011.

[33] X. Qiang, F.S.K. Bijlaard, H. Kolstein, Post-fire mechanical properties of high strength structural steels S460 and S690, Eng. Stru. 35 (2012) 1–10.

[34] A. Heidarpour, N.S. Tofts, A.H. Korayem, X.L. Zhao, C.R. Hutchinson, Mechanical properties of very high strength steel at elevated temperatures, Fire Saf. J. 64 (2014) 27–35.